Type II Seesaw Mechanism with Scalar Dark Matter in Light of AMS-02, DAMPE, and Fermi-LAT Data

T. Li – Nankai University

N. Okada – University of Alabama

Q. Shafi – University of Delaware

Citation of published version:

Li, T., Okada, N., Shafi, Q. (2018): Type II Seesaw Mechanism with Scalar Dark Matter in Light of AMS-02, DAMPE, and Fermi-LAT Data. *Physical Review D,* 98(5).
DOI: https://doi.org/10.1103/PhysRevD.98.055002

Type II seesaw mechanism with scalar dark matter in light of AMS-02, DAMPE, and Fermi-LAT data

Tong Li,[1] Nobuchika Okada,[2] and Qaisar Shafi[3]

[1]*School of Physics, Nankai University, Tianjin 300071, China*
[2]*Department of Physics and Astronomy, University of Alabama, Tuscaloosa, Alabama 35487, USA*
[3]*Bartol Research Institute, Department of Physics and Astronomy, University of Delaware, Newark, Delaware 19716, USA*

(Received 29 June 2018; published 4 September 2018)

The standard model (SM) supplemented by type II seesaw and a SM gauge-singlet scalar dark matter (DM) is a very simple framework to incorporate the observed neutrino oscillations and provide a plausible DM candidate. In this framework, the scalar DM naturally has a leptophilic nature with a pair annihilating mainly into the SM $SU(2)_L$ triplet Higgs scalar of type II Seesaw which, in turn, decay into leptons. In this work, we consider indirect signatures of this leptophilic DM and examine the spectrum of the cosmic ray electron/positron flux from DM pair annihilations in the Galactic halo. Given an astrophysical background spectrum of the cosmic ray electron/positron flux, we find that the contributions from DM annihilations can nicely fit the observed data from the AMS-02, DAMPE and Fermi-LAT collaborations, with a multi-TeV range of DM mass and a boost factor for the DM annihilation cross section of $\mathcal{O}(1000)$. The boost factor has a tension with the Fermi-LAT data for gamma-ray from dwarf spheroidal galaxies and the limit from CMB anisotropies, which can be ameliorated with enhanced local DM density by a factor of about two.

DOI: 10.1103/PhysRevD.98.055002

I. INTRODUCTION

The existence of dark matter (DM) in the Universe has been established by a variety of cosmological and astronomical observations. The nature of DM is still unknown and stands as one of the biggest mysteries in particle physics and cosmology. The measurements of Galactic cosmic rays can provide indirect information of DM particles since their pair annihilations or late-time decays produce cosmic rays such as cosmic ray positrons and antiprotons. As cosmic ray observations become more and more precise, a deviation (excess) of an observed cosmic ray flux from its astrophysical prediction can be used to learn about the nature of DM particles. The latest and most precise measurements of the cosmic ray electron and positron (CRE) flux have been reported by the AMS-02 [1], DAMPE [2], and Fermi-LAT [3] collaborations. The increase of the positron spectrum above 100 GeV and the break of the CRE spectrum around 1 TeV are unexpected results from these measurements, possibly indicating an excess of the CREs originating from DM particles.

In this paper, we consider a very simple extension of the standard model (SM), which simultaneously resolves two major missing pieces in the SM, namely, a dark matter candidate and a neutrino mass matrix compatible with the observed neutrino oscillations. This model was first proposed in Ref. [4] to account for an excess of cosmic ray positions reported by the PAMELA collaboration [5]. After the first results of the AMS-02 [6], detailed analysis for the cosmic ray position fluxes was performed in Ref. [7]. This and similar models were also adopted to explain the line-like $e^+ + e^-$ excess around 1.4 TeV, recently reported by the DAMPE [8–11]. In the model, a SM gauge-singlet real scalar (D) is introduced along with an unbroken Z_2 symmetry. The real scalar, which is a unique Z_2-odd field in the model, serves as the DM. In addition to the scalar DM, a SM $SU(2)_L$ triplet scalar field (Δ) is introduced to accommodate the observed neutrino oscillation phenomena [12] via the type II seesaw mechanism [13–17]. Through a four-point interaction between the DM and triplet scalars, a pair of the DM particles mainly annihilates into a pair of the triplet scalars, whose subsequent decays generate leptonic final states as a new source of CREs in the Galactic halo. The leptophilic nature of this DM particle is attributed to the type II seesaw mechanism. The main purpose of this paper is to revisit the CRE spectrum for the type II seesaw model extended with scalar DM and identify a parameter region to fit the latest CRE spectrum measured by the AMS-02, DAMPE, and Fermi-LAT collaborations.

This paper is organized as follows. In Sec. II, we describe the source and propagation of cosmic rays in the Galaxy including the DM contribution. In Sec. III we discuss the type II seesaw model with scalar DM and its contribution to electron/positron cosmic rays. Our numerical results of best-fit parameters in this model are given in Sec. IV, and we summarize our conclusions in Sec. V.

II. ELECTRON/POSITRON COSMIC RAYS IN THE GALAXY

The key unknowns about cosmic rays in the Galaxy are their origin and propagation. Primary cosmic rays originate from astrophysical processes, such as supernova explosions or pulsars. Their collisions with intergalactic matter create secondary cosmic rays. The propagation of cosmic rays can be described by the process of diffusion, in the form of the transport equation [18]:

$$\frac{\partial \psi}{\partial t} = Q(\vec{r}, p) + \vec{\nabla} \cdot (D_{xx} \vec{\nabla} \psi - \vec{V} \psi) + \frac{\partial}{\partial p} p^2 D_{pp} \frac{\partial}{\partial p} \frac{1}{p^2} \psi - \frac{\partial}{\partial p} \left[\dot{p} \psi - \frac{p}{3} (\vec{\nabla} \cdot \vec{V}) \psi \right] - \frac{\psi}{\tau_f} - \frac{\psi}{\tau_r}, \quad (1)$$

where $\psi(\vec{r}, t, p)$ is the density of cosmic rays, $\vec{V}$ is the convection velocity, $\tau_f(\tau_r)$ is the timescale for fragmentation (radioactive decay), and $\dot{p}$ is the momentum loss rate. In the above equation, the convection terms are governed by the Galactic wind and the diffusion in momentum space induces the reacceleration process. The spatial diffusion coefficient can then be written as

$$D_{xx} = \beta D_0 (R/R_0)^{\delta}, \quad (2)$$

with R and β being the rigidity and a particle velocity in unit of the speed of light, respectively. This transport equation is numerically solved with given boundary conditions, that is, the cosmic ray density ψ vanishes at the radius R_h and the height $\pm L$ of the cylindrical diffusion zone in the Galactic halo. The cosmic ray flux is then given by $\mathbf{v}\psi/(4\pi)$ with $\mathbf{v}$ being the cosmic ray velocity.

The source term in Eq. (1) for the primary cosmic rays can generally be given by the product of the spatial distribution and the injection spectrum function:

$$Q_i(\vec{r}, p) = f(r, z) q(p). \quad (3)$$

For the above spatial distribution, we use the following supernova remnants distribution,

$$f(r, z) = f_0 \left(\frac{r}{r_\odot} \right)^a \exp\left(-b \frac{r - r_\odot}{r_\odot} \right) \exp\left(-\frac{|z|}{z_s} \right), \quad (4)$$

where $r_\odot = 8.5$ kpc is the distance between the Sun and the Galactic center, and the height of the Galactic disk is taken to be $z_s = 0.2$ kpc. The two parameters a and b are chosen to be 1.25 and 3.56, respectively [19]. For the injection spectra of various nuclei and primary electrons, one can assume broken power law function with one or more breaks and indices. These rigidity breaks and power law indices are the source injection parameters.

The secondary-to-primary ratio of cosmic ray nuclei (the Boron-to-Carbon ratio B/C) and the ratio of secondary isotopes (the Beryllium ratio $^{10}\mathrm{Be}/^{9}\mathrm{Be}$) are widely employed to constrain the cosmic ray propagation parameters [20–28], as they are respectively sensitive to the traveling path and the lifetime of cosmic rays in the Galaxy. The source injection parameters of cosmic ray nuclei and electrons can be constrained by the measured proton flux data and the low energy regions of the CRE spectra, respectively. Recently, the AMS-02 collaboration released abundant and precise data on the cosmic ray nuclei, e.g., proton [29], B/C [30], and Helium [31]. Combining the latest CRE and nuclei data with old data sets such as from CREAM [32] and PAMELA [33], one can constrain the propagation and source injection parameters in a statistical method. Based on these well fitted parameters, an up-to-date primary electron and secondary electron/positron cosmic rays can be obtained with high precision. Given this astrophysical background, at high energies, we are enabled to constrain extra compositions in cosmic rays such as annihilating dark matter which also produces electrons and positrons, in the light of the flux data newly reported by the AMS-02, DAMPE, and Fermi-LAT collaborations. In practice, we use the CRE background flux obtained in Ref. [34] (see also Ref. [35]) which takes into account the latest AMS-02 and DAMPE data based on the above global fitting procedure. We should keep in mind that both the explanation for the CRE excess measurements and the background modeling are the subject of debate. In addition to DM annihilation, there exist alternative astrophysical explanations for the difference between the data and prediction. The conclusion of the constraints on DM signal below is dependent on the background model adopted here.

The DM source term of the CREs for a self-conjugate DM particle can be described by the product of the spatial function and the spectrum distribution as follows

$$Q(r, p) = \frac{1}{2} \frac{\rho^2(r)}{m_D^2} \langle \sigma v \rangle \frac{dN}{dE}. \quad (5)$$

Here, $\rho(r)$ is the DM spatial distribution, $\langle \sigma v \rangle$ is the total velocity-averaged DM annihilation cross section, and dN/dE is the energy spectrum of cosmic ray particles produced by the DM annihilation. For the DM spatial distribution, we assume the standard Navarro-Frenk-White (NFW) profile [36,37] to describe DM halo within the Galaxy

$$\rho(r) = \rho_s \frac{(r/r_s)^{-\gamma}}{(1 + r/r_s)^{3-\gamma}}, \quad (6)$$

with $\gamma = 1$ and $r_s = 20$ kpc. The coefficient ρ_s is set to give the local DM density $\rho(r_\odot) = 0.4$ Gev/cm^3. The spectrum dN/dE depends on specific DM models.

III. TYPE II SEESAW MODEL WITH SCALAR DM

In Table I, we list the particle content of the type II seesaw model with scalar DM, relevant for our discussion in this paper. An odd parity under the unbroken Z_2 symmetry is assigned to the SM gauge-singlet scalar (D), which makes it stable and a suitable DM candidate. The explicit form of the SU(2)$_L$ triplet scalar in terms of three complex scalars (electric charge neutral (Δ^0), singly charged (Δ^+) and doubly charged (Δ^{++}) scalars) is given by

$$\Delta = \frac{\sigma^i}{\sqrt{2}}\Delta_i = \begin{pmatrix} \Delta^+/\sqrt{2} & \Delta^{++} \\ \Delta^0 & -\Delta^+/\sqrt{2} \end{pmatrix}, \tag{7}$$

where σ^i's are Pauli matrices.

Following the notations of Ref. [38], the scalar potential relevant for type II seesaw is given by

$$\begin{aligned} V(H,\Delta) = & -m_H^2(H^\dagger H) + \frac{\lambda}{2}(H^\dagger H)^2 \\ & + M_\Delta^2 \mathrm{tr}[\Delta^\dagger\Delta] + \frac{\lambda_1}{2}(\mathrm{tr}[\Delta^\dagger\Delta])^2 \\ & + \frac{\lambda_2}{2}((\mathrm{tr}[\Delta^\dagger\Delta])^2 - \mathrm{tr}[\Delta^\dagger\Delta\Delta^\dagger\Delta]) \\ & + \lambda_4 H^\dagger H \mathrm{tr}(\Delta^\dagger\Delta) + \lambda_5 H^\dagger[\Delta^\dagger,\Delta]H \\ & + [2\lambda_6 M_\Delta H^T i\sigma_2 \Delta^\dagger H + \mathrm{H.c.}], \end{aligned} \tag{8}$$

where the coupling constants λ_i are taken to be real without loss of generality. The scalar potential relevant for DM D is

$$V(D) = \frac{1}{2}m_0^2 D^2 + \lambda_D D^4 + \lambda_H D^2 H^\dagger H + \lambda_\Delta D^2 \mathrm{tr}(\Delta^\dagger\Delta). \tag{9}$$

TABLE I. Particle content of the type II seesaw model with scalar DM, relevant to our discussion in this paper. In addition to the SM lepton doublets ℓ_L^i ($i = 1, 2, 3$ being the generation index) and the Higgs doublet H, a complex SU(2)$_L$ triplet scalar Δ, and a SM gauge-singlet real scalar D are introduced, along with an unbroken Z_2 symmetry. The triplet scaler Δ plays a key role in type II seesaw mechanism, while the scalar D is the DM candidate.

	SU(2)$_L$	U(1)$_Y$	Z_2
ℓ_L^i	**2**	$-1/2$	$+$
H	**2**	$+1/2$	$+$
Δ	**3**	$+1$	$+$
D	**1**	0	$-$

Through the couplings λ_H and λ_Δ in this scalar potential, a pair of scalar DM particles annihilates into pairs of the Higgs doublet and the triplet, i.e., $DD \to H^\dagger H$, $\Delta^\dagger\Delta$. nonzero vacuum expectation value (VEV) of the Higgs doublet (v) generates a tadpole term for Δ through the last term in Eq. (8). Minimizing the scalar potential, we obtain a nonzero VEV of the triplet Higgs as $\langle\Delta^0\rangle = v_\Delta/\sqrt{2} \simeq \lambda_6 v^2/M_\Delta$, by which the lepton number is spontaneously broken. In order to achieve the right scale of the electroweak symmetry breaking, the constraint, $v^2 + v_\Delta^2 = (246\ \mathrm{GeV})^2$, must be satisfied. After the electroweak symmetry breaking, one has the following triplet masses in the limit of $v \gg v_\Delta$,

$$\begin{aligned} M_{\Delta^{\pm\pm}}^2 &= M_\Delta^2 + \frac{1}{2}(\lambda_4+\lambda_5)v^2, \qquad M_{\Delta^\pm}^2 = M_\Delta^2 + \frac{1}{2}\lambda_4 v^2, \\ M_{\Delta^0}^2 &= M_\Delta^2 + \frac{1}{2}(\lambda_4-\lambda_5)v^2. \end{aligned} \tag{10}$$

Here, Δ^0 represents both CP-even and CP-odd neutral triplet Higgs bosons. Taking a negative value for λ_5, we can arrange a nondegenerate spectrum for the triplet Higgs bosons with only the doubly charged Higgs boson being lighter than the scalar DM particle, i.e., $M_{\Delta^{\pm\pm}} < m_D < M_{\Delta^\pm}, M_{\Delta^0}$. In this case, through Eq. (9), a pair of scalar DM particles annihilates only into a pair of doubly charged Higgs bosons with a cross section

$$\langle\sigma v\rangle(DD \to \Delta^{++}\Delta^{--}) = \frac{1}{8\pi m_D^2}\lambda_\Delta^2\sqrt{1 - \frac{M_{\Delta^{\pm\pm}}^2}{m_D^2}}. \tag{11}$$

Here we assume $\lambda_H \ll \lambda_\Delta$ to accommodate the direct DM detection [9] and thus forbid annihilation into the Higgs doublet. Although the small λ_H leads to negligible DM-nucleon scattering mediated by the SM Higgs boson in the t-channel, there exist loop diagrams induced by the quartic coupling λ_Δ for direct detection. These penguinlike diagrams arise from the loop exchange of charged triplet Higgses and γ/Z bosons. They generate the nonvanishing scattering operator $D^2\bar{q}\gamma_5 q$, which leads to a momentum-suppressed spin-dependent cross section [39]. As a result, together with the suppression by the heavy triplet Higgses in the loop, the relevant scattering cross section would not be within reach of current or forthcoming experiments such as XENON nT or LZ. Since the annihilation modes into neutral and singly charged Higgs bosons are forbidden, neutrinos are not created from the prompt decay of the triplet scalar, thus evading a possible constraint from the IceCube experiment [40,41].

As in the canonical type II seesaw, the triplet scalar (Δ) has a Yukawa coupling with the lepton doublets given by

$$\mathcal{L}_\Delta = -\frac{1}{\sqrt{2}}(Y_\Delta)_{ij}(\ell_L^i)^T C i\sigma_2 \Delta \ell_L^j + \text{H.c.}$$
$$= -\frac{1}{\sqrt{2}}(Y_\Delta)_{ij}(\nu_L^i)^T C \Delta^0 \nu_L^j + \frac{1}{2}(Y_\Delta)_{ij}(\nu_L^i)^T C \Delta^+ e_L^j$$
$$+ \frac{1}{\sqrt{2}}(Y_\Delta)_{ij}(e_L^i)^T C \Delta^{++} e_L^j + \text{H.c.}, \quad (12)$$

where C is the charge conjugate matrix, and $(Y_\Delta)_{ij}$ denotes the elements of the Yukawa matrix. In Eq. (12), the neutrino mass matrix is given by

$$m_\nu = v_\Delta (Y_\Delta)_{ij}. \quad (13)$$

The Yukawa interactions of the doubly charged Higgs boson are

$$\mathcal{L}_\Delta \supset -\frac{1}{\sqrt{2}}(e_L^i)^T C (Y_\Delta)_{ij} \Delta^{++} e_L^j, \quad (14)$$

and the partial decay width of the doubly charged Higgs boson into a same-sign dilepton is thus given by

$$\Gamma(\Delta^{++} \to i^+ j^+) = \frac{1}{8\pi(1+\delta_{ij})}|(Y_\Delta)_{ij}|^2 M_{\Delta^{++}},$$
$$i, j = e, \mu, \tau. \quad (15)$$

For $v_\Delta \lesssim 10^{-4}$ GeV, the decays of doubly charged Higgs are dominated by the above leptonic channels [42]. With this assumption we focus only on the same-sign leptonic decay modes of Δ^{++} in the analysis below. Thus, the decay branching ratios are only governed by Eq. (15) and are independent of the triplet Higgs mass. Note that the Yukawa coupling matrix Y_Δ has a direct relation with the neutrino oscillation data,

$$Y_\Delta = \frac{1}{v_\Delta} U_{\text{PMNS}}^* D_\nu U_{\text{PMNS}}^\dagger, \quad (16)$$

with U_{PMNS} being the Pontecorvo-Maki-Nakagawa-Sakata (PMNS) neutrino mixing matrix and D_ν is a diagonal mass eigenvalue matrix for the light neutrinos. Using the neutrino oscillation data [12] and the above decay width formula, we can obtain the patterns of the charged lepton flavors produced by the doubly charged Higgs boson decay. In the following numerical calculations, we consider two cases for the light neutrino mass spectrum, namely, the normal hierarchy (NH) and the inverted hierarchy (IH) to account for the undetermined neutrino mass ordering. For the two benchmarks, the obtained branching ratios of the doubly charged Higgs boson decay into the leptonic final states are shown in Table II [43]. Remarkably, the branching ratio of doubly charged Higgs decay into $e^\pm e^\pm$ in IH is 50 times greater than that in NH, while all remaining decay channels are comparable between these two mass patterns.

TABLE II. Benchmark decay branching ratios of doubly charged Higgs boson for NH and IH spectra.

BR	ee	$e\mu$	$e\tau$	$\mu\mu$	$\mu\tau$	$\tau\tau$
NH	1%	2%	2%	30%	35%	30%
IH	50%	1%	1%	12%	24%	12%

For the 4-body CRE spectrum we consider, one has

$$\frac{dN}{dE} = \sum_{i,j} \text{BR}(\Delta^{\pm\pm} \to i^\pm j^\pm)\left(\frac{d\bar{N}_i}{dE} + \frac{d\bar{N}_j}{dE}\right), \quad (17)$$

where $i, j = e, \mu, \tau$. The cosmic ray spectrum $d\bar{N}/dE$ in the lab frame is given by the spectrum from the triplet Higgs decay in its rest frame, denoted by dN/dE_0, after a Lorentz boost [44,45]. Namely,

$$\frac{d\bar{N}}{dE} = \int_{t_{1,\min}}^{t_{1,\max}} \frac{dx_0}{x_0\sqrt{1-\epsilon^2}}\frac{dN}{dE_0}, \quad (18)$$

where

$$t_{1,\max} = \min\left[1, \frac{2x}{\epsilon^2}\left(1+\sqrt{1-\epsilon^2}\right)\right], \quad (19)$$

$$t_{1,\min} = \frac{2x}{\epsilon^2}\left(1-\sqrt{1-\epsilon^2}\right), \quad (20)$$

with $\epsilon = M_{\Delta^{\pm\pm}}/m_D$ and $x = E/m_D \leq 0.5$. For the propagation parameters of dark matter, we assume the MED model [46,47] with $\delta = 0.7$, $D_0 = 0.0112$ kpc^2/Myr, $L = 4$ kpc and the convective velocity $V_C = 12$ km/s, and use MicrOMEGAs 5.0 [48] to calculate the CRE spectrum from DM annihilations.

IV. RESULTS

The obtained cosmic ray fluxes, together with the experimental data points, are put into a composite likelihood function, defined as

$$\chi^2 = \sum_i \frac{(f_i^{\text{th}} - f_i^{\text{exp}})^2}{\sigma_i^2}, \quad (21)$$

where $f_i^{\text{th}} = f_i^{\text{DM}} + f_i^{\text{bkg}}$ are the theoretical predictions of the CRE flux from the DM annihilation (f_i^{DM}) plus the astronomical background (f_i^{bkg}), while f_i^{exp} are the corresponding central value of the experimental data. In order to take into account, amongst others, the uncertainty related to the fixed propagation parameters, we stipulate a 10% uncertainty of the theoretical predictions. The theoretical and experimental uncertainties are then combined in quadrature to yield the σ_i. The sum in Eq. (21) runs over the AMS-02 e^+ flux data ($E > 1$ GeV, 70 data points), the

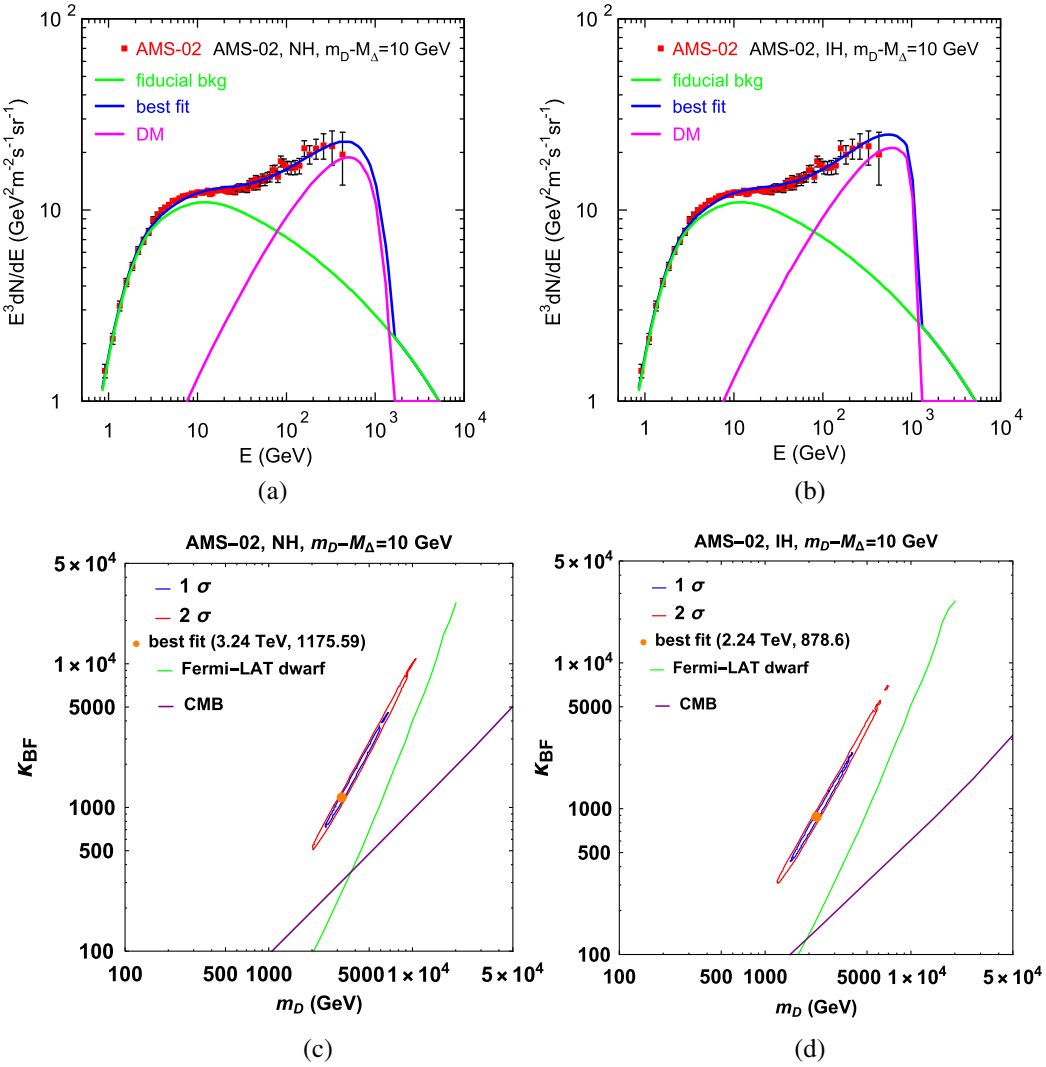

FIG. 1. (a) and (b): Comparison of the positron flux observed by the AMS-02 (red dots and dark error bars) with the type II seesaw model with scalar dark matter, for $m_D - M_{\Delta^{++}} = 10$ GeV, and NH (a) and IH (b) spectra. The blue solid line shows the prediction of the total cosmic ray flux with dark matter parameter values that best fit the AMS-02 data. The total predicted flux is the sum of the background flux (green curve) and the dark matter contribution (purple curve). (c) and (d): The AMS-02 favored region and best-fit point (orange point) of DM model parameters ($\kappa_{\rm BF}$ vs m_D), for $m_D - M_{\Delta^{++}} = 10$ GeV, and NH (c) and IH (d) spectra. The contours represent 1σ (blue) and 2σ (red) confidence regions. The upper limits on $\kappa_{\rm BF}$ by the Fermi-LAT (green curve) and CMB (purple curve) are also shown.

DAMPE $e^+ + e^-$ data (without the excess point at $E \simeq 1.4$ TeV, 37 data points) or the Fermi-LAT $e^+ + e^-$ data (High-Energy region with $E > 42$ GeV, 27 data points). Note that, for the DAMPE data, we exclude the data point with energy of about 1.4 TeV, as the evidence for the kneelike feature of $e^+ + e^-$ is rather strong but the linelike signal has to be confirmed in the future [49].

Due to the nondegenerate spectrum for triplet Higgs, we assume a mass benchmark with small difference $m_D - M_{\Delta^{++}} = 10$ GeV, and $\langle\sigma v\rangle = \kappa_{\rm BF}\langle\sigma v\rangle_0$ with $\langle\sigma v\rangle_0 = 3 \times 10^{-26}$ cm^3/s (typical thermal DM annihilation cross section) and $\kappa_{\rm BF}$ being the boost factor. Thus, we employ two free parameters, m_D and $\kappa_{\rm BF}$, to fit the observed CRE spectrum. Note that, although the small mass difference gives a phase-space suppression factor for the annihilation rate, the quartic coupling λ_Δ remains in the perturbative range [9]. In Figs. 1(a) and 1(b), we display our best-fit spectrum of cosmic ray positron in the type II seesaw with scalar DM, for $m_D - M_{\Delta^{++}} = 10$ GeV, and NH and IH spectra, along with the AMS-02 data. Figures 1(c) and 1(d) also shows the favored region and the best-fit point of the DM model parameters in the plane of $\kappa_{\rm BF}$ vs m_D to fit the AMS-02 data. In Figs. 2 and 3, we show our results corresponding to Fig. 1 but for fitting the $e^+ + e^-$ flux measured by the DAMPE and the Fermi-LAT collaborations, respectively. The corresponding favored regions and the best-fit points of the DM model parameters are also shown. Figure 4 displays the favored regions and

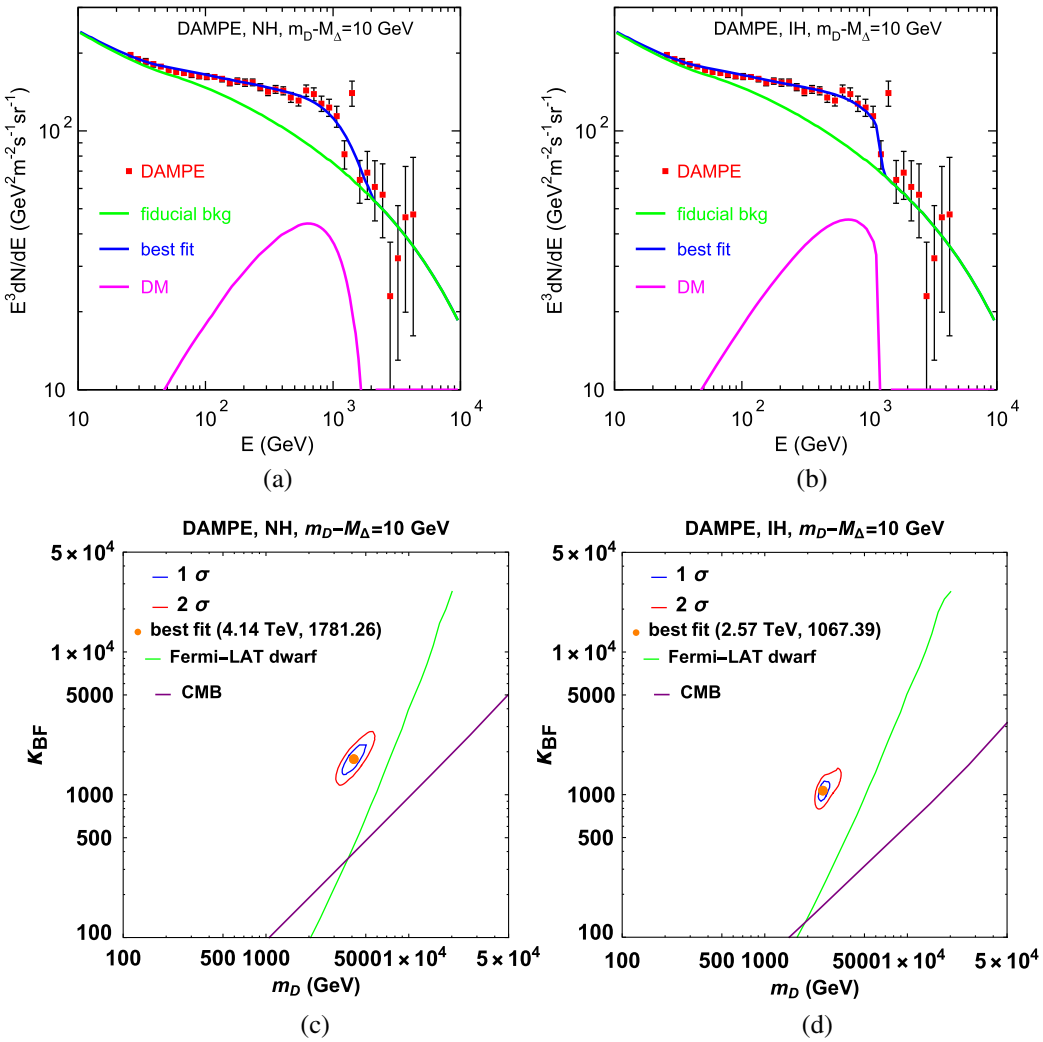

FIG. 2. Electron plus positron flux that best fit the DAMPE data, as labeled in Fig. 1.

the best-fit points by combined AMS-02, DAMPE, and Fermi-LAT. Our results indicate that these CRE observations are consistent with the dark matter hypothesis by improving the fit to the data.

Our results of best-fit parameters are summarized in Table III. One can see that the increase of e^+ or $e^+ + e^-$ favors a multi-TeV DM mass and a boost factor $\kappa_{\rm BF} = \mathcal{O}(1000)$ for the annihilation cross section in this model. The Breit-Wigner enhancement for boosting the annihilation cross section of the DM particles may arise by introducing a new scalar coupled to D and Δ [4,9]. In particular, with 50 times greater branching ratio of doubly charged Higgs decay into $e^{\pm}e^{\pm}$, the favored DM mass in IH has a reduction of $30\% - 40\%$ compared to that in NH. It is due to the sharper spectrum induced by the leading prompt $e^{\pm}e^{\pm}$ channel in IH. Moreover, as the first direct detection of $e^+ + e^-$ knee, DAMPE relatively prefers IH over NH, while both of NH and IH in this model indistinguishably fit AMS-02 and Fermi-LAT without a measured kneelike feature. More precise measurement of the flux for higher energy range in the future should reveal a preference for NH or IH.

With a large amount of dark matter, dwarf galaxies serve as the bright targets for searching gamma rays from dark matter annihilation. Since the Fermi-LAT experiments [50,51] have found no gamma ray excess from the dwarf spheroidal satellite galaxies (dSphs) of the Milky Way, following the Fermi's maximum likelihood analysis, one can place an upper limit on the DM annihilation cross section for a given m_D. This limit appears to be more stringent than other gamma ray observations from the Milky Way [50]. We perform the likelihood analysis and show the upper limit on $\kappa_{\rm BF}$ by the Fermi-LAT dSphs in Figs. 1–3. One can see a tension between the CRE favored region and the Fermi-LAT dSphs limit. An enhancement by a factor of about two of the local DM density is needed to evade the Fermi-LAT dSphs constraint. This enhancement can be ascribed to density fluctuations in the Milky Way halo [52]. The observations of cosmic microwave background (CMB) anisotropies also provide constraint on this

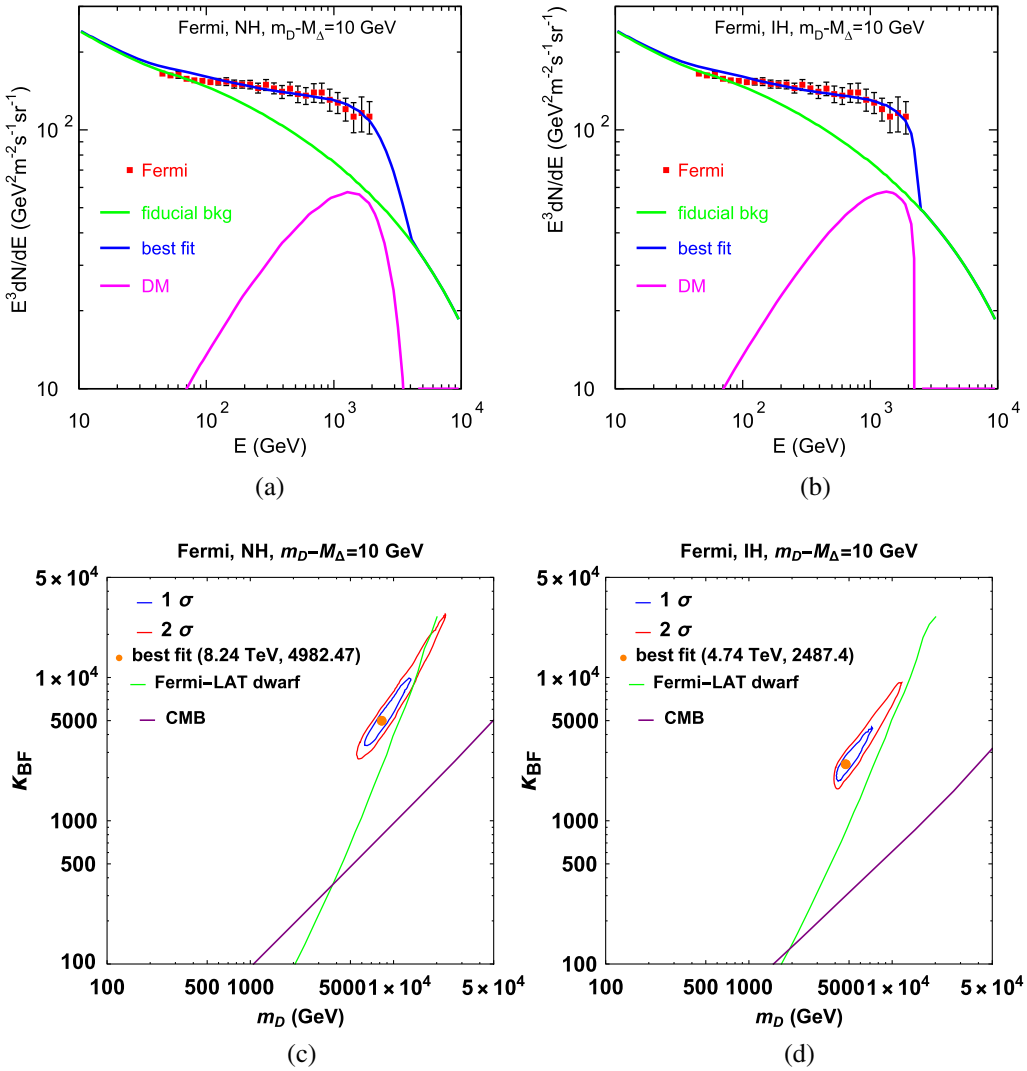

FIG. 3. Electron plus positron flux that best fit the Fermi-LAT data, as labeled in Fig. 1.

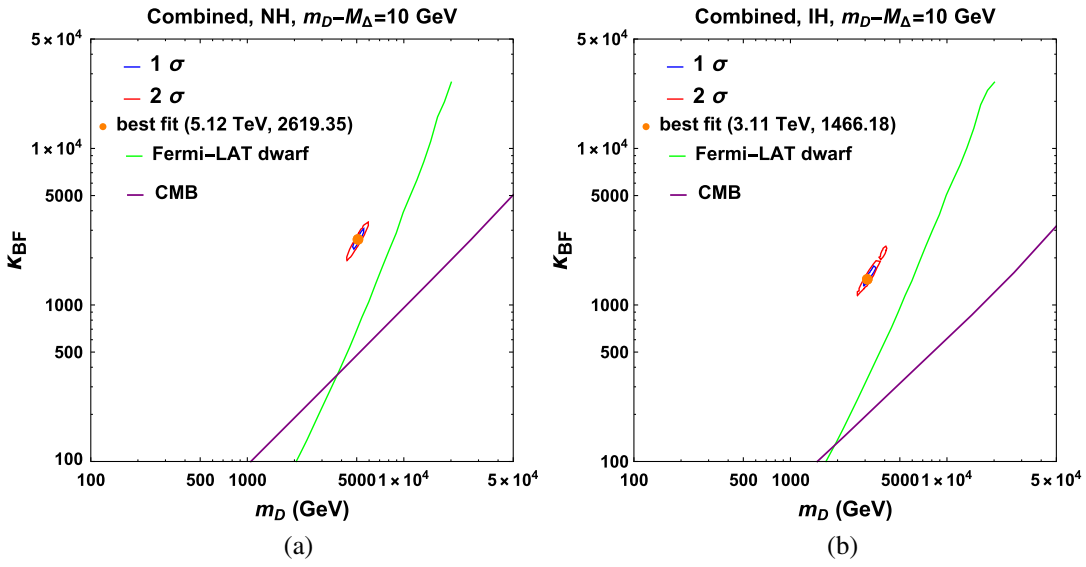

FIG. 4. The favored region and best-fit point by combined AMS-02, DAMPE and Fermi-LAT, as labeled in Fig. 1.

TABLE III. Best-fit m_D, $\kappa_{\rm BF}$ and $\chi^2_{\rm min}$ for the NH and IH mass spectra, by AMS-02, DAMPE, and Fermi-LAT, assuming $m_D - M_{\Delta^{++}} = 10$ GeV.

Best-fit m_D, $\kappa_{\rm BF}$	AMS-02	DAMPE	Fermi-LAT	Combined
NH	3.24 TeV, 1175.6	4.14 TeV, 1781.3	8.24 TeV, 4982.5	5.12 TeV, 2619.4
	$\chi^2_{\rm min} = 9.9$	$\chi^2_{\rm min} = 7.2$	$\chi^2_{\rm min} = 2.73$	$\chi^2_{\rm min} = 35.1$
IH	2.24 TeV, 878.6	2.57 TeV, 1067.4	4.74 TeV, 2487.4	3.11 TeV, 1466.2
	$\chi^2_{\rm min} = 10.0$	$\chi^2_{\rm min} = 5.53$	$\chi^2_{\rm min} = 2.83$	$\chi^2_{\rm min} = 47.9$

model with annihilating DM [53]. From Planck temperature and polarization data, the bound is taken to be [54]

$$\frac{\langle\sigma v\rangle f_{\rm eff}}{m_D} < 4.1 \times 10^{-28}\ {\rm cm}^3/{\rm s/GeV}, \tag{22}$$

where $f_{\rm eff}$ is an efficiency factor determined by the spectrum of injected electrons and photons from prompt DM annihilation into lepton species in Eq. (17). Given the efficiency curve as a function of energy for e^+/e^- and photons in Ref. [55], we obtain the CMB upper limit on $\kappa_{\rm BF}$ as shown in the bottom panels of Figs. 1–3. The enhancement factor of about two of the local DM density can also help to evade the CMB constraint.

V. CONCLUSION

Type II seesaw extension of the SM with a SM gauge-singlet scalar DM is a simple framework to supplement the SM with the desired neutrino mass matrix and a plausible DM candidate. With a suitable choice of the model parameters, the scalar DM naturally becomes leptophilic; a pair of DM particles mainly annihilates into the doubly charged Higgs bosons which, in turn, decay into charged leptons. We have calculated the spectrum of the cosmic ray electron/positron flux from DM pair annihilations in the Galactic halo. Given an astrophysical background spectrum of the cosmic ray flux, we have found that the contributions from the DM annihilations can nicely fit the cosmic ray spectrum measured by the AMS-02, DAMPE, and Fermi-LAT collaborations, with a multi-TeV range of DM mass and a boost factor for the DM annihilation cross section of $\mathcal{O}(1000)$. Because of the type II seesaw structure for generating the neutrino mass matrix, the lepton flavor decomposition of the primary leptons from the doubly charged Higgs boson decay is determined by the pattern of the light neutrino mass spectrum and the neutrino oscillations data. We have considered the NH and IH cases for the light neutrino mass spectrum. As summarized in Table III, the IH case is preferred for fitting the DAMPE data, while both the NH and IH cases can equally fit the AMS-02 and the Fermi-LAT data. We have also considered the Fermi-LAT and CMB constraints on the DM pair annihilation cross section and found a tension, which can be ameliorated with an enhanced local DM density by a factor of about two.

ACKNOWLEDGMENTS

This work is supported in part by the DOE Grants No. DE-SC0012447 (N. O.) and DE-SC0013880 (Q. S.).

[1] M. Aguilar *et al.* (AMS Collaboration), Electron and Positron Fluxes in Primary Cosmic Rays Measured with the Alpha Magnetic Spectrometer on the International Space Station, Phys. Rev. Lett. **113**, 121102 (2014).
[2] G. Ambrosi *et al.* (DAMPE Collaboration), Direct detection of a break in the teraelectronvolt cosmic-ray spectrum of electrons and positrons, Nature (London) **552**, 63 (2017).
[3] S. Abdollahi *et al.* (Fermi-LAT Collaboration), Cosmic-ray electron-positron spectrum from 7 GeV to 2 TeV with the Fermi Large Area Telescope, Phys. Rev. D **95**, 082007 (2017).
[4] I. Gogoladze, N. Okada, and Q. Shafi, Type II seesaw and the PAMELA/ATIC signals, Phys. Lett. B **679**, 237 (2009).
[5] O. Adriani *et al.* (PAMELA Collaboration), An anomalous positron abundance in cosmic rays with energies 1.5–100 GeV, Nature (London) **458**, 607 (2009).
[6] M. Aguilar *et al.* (AMS Collaboration), First Result from the Alpha Magnetic Spectrometer on the International Space Station: Precision Measurement of the Positron Fraction in Primary Cosmic Rays of 0.5350 GeV, Phys. Rev. Lett. **110**, 141102 (2013).
[7] P. S. B. Dev, D. K. Ghosh, N. Okada, and I. Saha, Neutrino mass and dark matter in light of recent AMS-02 results, Phys. Rev. D **89**, 095001 (2014).
[8] C. H. Chen, C. W. Chiang, and T. Nomura, Explaining the DAMPE e^+e^- excess using the Higgs triplet model with a vector dark matter, Phys. Rev. D **97**, 061302 (2018).
[9] T. Li, N. Okada, and Q. Shafi, Scalar dark matter, type II Seesaw and the DAMPE cosmic ray $e^+ + e^-$ excess, Phys. Lett. B **779**, 130 (2018).

[10] Y. Sui and Y. Zhang, Prospects of type-II seesaw at future colliders in light of the DAMPE e^+e^- excess, Phys. Rev. D **97**, 095002 (2018).
[11] J. Cao, X. Guo, L. Shang, F. Wang, P. Wu, and L. Zu, Scalar dark matter explanation of the DAMPE data in the minimal left-right symmetric model, Phys. Rev. D **97**, 063016 (2018).
[12] C. Patrignani *et al.* (Particle Data Group), Review of particle physics, Chin. Phys. C **40**, 100001 (2016).
[13] G. Lazarides, Q. Shaf,i, and C. Wetterich, Proton lifetime and fermion masses in an SO(10) model, Nucl. Phys. **B181**, 287 (1981).
[14] R. N. Mohapatra and G. Senjanovic, Neutrino masses and mixings in gauge models with spontaneous parity violation, Phys. Rev. D **23**, 165 (1981).
[15] M. Magg and C. Wetterich, Neutrino mass problem and gauge hierarchy, Phys. Lett. **94B**, 61 (1980).
[16] J. Schechter and J. W. F. Valle, Neutrino masses in $SU(2) \times U(1)$ theories, Phys. Rev. D **22**, 2227 (1980).
[17] For recent review on Type II Seesaw, see, e.g., M. Lindner, M. Platscher, and F. S. Queiroz, A call for new physics: The muon anomalous magnetic moment and lepton flavor violation, Phys. Rep. **731**, 1 (2018); Y. Cai, T. Han, T. Li, and R. Ruiz, Lepton-number violation: Seesaw models and their collider tests, Front. Phys. **6**, 40 (2018).
[18] A. W. Strong, I. V. Moskalenko, and V. S. Ptuskin, Cosmic-ray propagation and interactions in the Galaxy, Annu. Rev. Nucl. Part. Sci. **57**, 285 (2007).
[19] R. Trotta, G. Johannesson, I. V. Moskalenko, T. A. Porter, R. R. de Austri, and A. W. Strong, Constraints on cosmic-ray propagation models from a global Bayesian analysis, Astrophys. J. **729**, 106 (2011).
[20] S. J. Lin, Q. Yuan, and X. J. Bi, Quantitative study of the AMS-02 electron/positron spectra: Implications for pulsars and dark matter properties, Phys. Rev. D **91**, 063508 (2015).
[21] A. Cuoco, M. Krämer, and M. Korsmeier, Novel Dark Matter Constraints from Antiprotons in Light of AMS-02, Phys. Rev. Lett. **118**, 191102 (2017).
[22] M. Y. Cui, Q. Yuan, Y. L. S. Tsai, and Y. Z. Fan, Possible Dark Matter Annihilation Signal in the AMS-02 Antiproton Data, Phys. Rev. Lett. **118**, 191101 (2017).
[23] J. Feng, N. Tomassetti, and A. Oliva, Bayesian analysis of spatial-dependent cosmic-ray propagation: Astrophysical background of antiprotons and positrons, Phys. Rev. D **94**, 123007 (2016).
[24] X. J. Huang, C. C. Wei, Y. L. Wu, W. H. Zhang, and Y. F. Zhou, Antiprotons from dark matter annihilation through light mediators and a possible excess in AMS-02 $\bar{p}/p$ data, Phys. Rev. D **95**, 063021 (2017).
[25] S. J. Lin, X. J. Bi, J. Feng, P. F. Yin, and Z. H. Yu, A systematic study on the cosmic ray antiproton flux, Phys. Rev. D **96**, 123010 (2017).
[26] H. B. Jin, Y. L. Wu, and Y. F. Zhou, Astrophysical background and dark matter implication based on latest AMS-02 data, arXiv:1701.02213.
[27] Q. Yuan, S. J. Lin, K. Fang, and X. J. Bi, Propagation of cosmic rays in the AMS-02 era, Phys. Rev. D **95**, 083007 (2017).
[28] J. S. Niu and T. Li, Galactic cosmic-ray model in the light of AMS-02 nuclei data, Phys. Rev. D **97**, 023015 (2018).
[29] M. Aguilar *et al.* (AMS Collaboration), Precision Measurement of the Proton Flux in Primary Cosmic Rays from Rigidity 1 GV to 1.8 TV with the Alpha Magnetic Spectrometer on the International Space Station, Phys. Rev. Lett. **114**, 171103 (2015).
[30] M. Aguilar *et al.* (AMS Collaboration), Precision Measurement of the Boron to Carbon Flux Ratio in Cosmic Rays from 1.9 GV to 2.6 TV with the Alpha Magnetic Spectrometer on the International Space Station, Phys. Rev. Lett. **117**, 231102 (2016).
[31] M. Aguilar *et al.* (AMS Collaboration), Precision Measurement of the Helium Flux in Primary Cosmic Rays of Rigidities 1.9 GV to 3 TV with the Alpha Magnetic Spectrometer on the International Space Station, Phys. Rev. Lett. **115**, 211101 (2015).
[32] Y. S. Yoon *et al.*, Cosmic-ray proton and helium spectra from the first CREAM flight, Astrophys. J. **728**, 122 (2011).
[33] O. Adriani *et al.*, Time dependence of the proton flux measured by PAMELA during the July 2006—December 2009 solar minimum, Astrophys. J. **765**, 91 (2013).
[34] J. S. Niu, T. Li, R. Ding, B. Zhu, H. F. Xue, and Y. Wang, Bayesian analysis of the DAMPE lepton spectra and two simple model interpretations, Phys. Rev. D **97**, 083012 (2018).
[35] S. F. Ge, H. J. He, and Y. C. Wang, Flavor structure of the cosmic-ray electron/positron excesses at DAMPE, Phys. Lett. B **781**, 88 (2018).
[36] J. F. Navarro, C. S. Frenk, and S. D. M. White, The structure of cold dark matter halos, Astrophys. J. **462**, 563 (1996).
[37] J. F. Navarro, C. S. Frenk, and S. D. M. White, A universal density profile from hierarchical clustering, Astrophys. J. **490**, 493 (1997).
[38] M. A. Schmidt, Renormalization group evolution in the type I + II seesaw model, Phys. Rev. D **76**, 073010 (2007); Erratum **85**, 099903 (2012).
[39] J. Kumar and D. Marfatia, Matrix element analyses of dark matter scattering and annihilation, Phys. Rev. D **88**, 014035 (2013).
[40] M. G. Aartsen *et al.* (IceCube Collaboration), The IceCube Neutrino Observatory—Contributions to ICRC 2017 Part I: Searches for the sources of astrophysical neutrinos, arXiv:1710.01179.
[41] Y. Zhao, K. Fang, M. Su, and M. C. Miller, A strong test of the dark matter origin of the 1.4 TeV DAMPE signal using IceCube neutrinos, J. Cosmol. Astropart. Phys. 06 (2018) 030.
[42] P. F. Perez, T. Han, G. Y. Huang, T. Li, and K. Wang, Testing a neutrino mass generation mechanism at the LHC, Phys. Rev. D **78**, 071301 (2008); , Neutrino masses and the CERN LHC: Testing type II seesaw, Phys. Rev. D **78**, 015018 (2008).
[43] T. Li, Type II Seesaw and tau lepton at the HL-LHC, HE-LHC and FCC-hh, arXiv:1802.00945.
[44] G. Elor, N. L. Rodd, and T. R. Slatyer, Multistep cascade annihilations of dark matter and the Galactic center excess, Phys. Rev. D **91**, 103531 (2015).
[45] G. Elor, N. L. Rodd, T. R. Slatyer, and W. Xue, Model-independent indirect detection constraints on hidden sector dark matter, J. Cosmol. Astropart. Phys. 06 (2016) 024.

[46] T. Delahaye, R. Lineros, F. Donato, N. Fornengo, and P. Salati, Positrons from dark matter annihilation in the galactic halo: Theoretical uncertainties, Phys. Rev. D **77**, 063527 (2008).

[47] F. Donato, N. Fornengo, D. Maurin, and P. Salati, Antiprotons in cosmic rays from neutralino annihilation, Phys. Rev. D **69**, 063501 (2004).

[48] G. Belanger, F. Boudjema, A. Goudelis, A. Pukhov, and B. Zaldivar, micrOMEGAs5.0: Freeze-in, Comput. Phys. Commun. **231**, 173 (2018).

[49] A. Fowlie, DAMPE squib? Significance of the 1.4 TeV DAMPE excess, Phys. Lett. B **780**, 181 (2018).

[50] M. Ackermann *et al.* (Fermi-LAT Collaboration), Searching for Dark Matter Annihilation from Milky Way Dwarf Spheroidal Galaxies with Six Years of Fermi Large Area Telescope Data, Phys. Rev. Lett. **115**, 231301 (2015).

[51] A. Drlica-Wagner *et al.* (Fermi-LAT and DES Collaborations), Search for gamma-ray emission from DES dwarf spheroidal galaxy candidates with Fermi-LAT data, Astrophys. J. **809**, L4 (2015).

[52] M. Kamionkowski, S. M. Koushiappas, and M. Kuhlen, Galactic substructure and dark matter annihilation in the Milky Way halo, Phys. Rev. D **81**, 043532 (2010).

[53] Q. Yuan *et al.*, Interpretations of the DAMPE electron data, arXiv:1711.10989.

[54] P. A. R. Ade *et al.* (Planck Collaboration), Planck 2015 results. XIII. Cosmological parameters, Astron. Astrophys. **594**, A13 (2016).

[55] T. R. Slatyer, Indirect dark matter signatures in the cosmic dark ages. I. Generalizing the bound on s-wave dark matter annihilation from Planck results, Phys. Rev. D **93**, 023527 (2016).